forests

MDPI

Article

Analysis of Linkage between Long-Term Morphological Spatial Pattern Analysis and Vegetation Carbon Storage of Forests in Hunan, China

Binglun Li [1,†], Longchi Chen [1,†], Qingkui Wang [1,2,*] and Peng Wang [1,*]

1 Huitong Experimental Station of Forest Ecology, CAS Key Laboratory of Forest Ecology and Management, Institute of Applied Ecology, Shenyang 110016, China; libinglun@iae.ac.cn (B.L.); lcchen@iae.ac.cn (L.C.)
2 School of Forestry & Landscape Architecture, Anhui Agricultural University, Hefei 230031, China
* Correspondence: wqkui@163.com (Q.W.); wangpeng@iae.ac.cn (P.W.)
† These authors contributed equally to this work.

Abstract: The carbon sequestration of forest ecosystems plays a pivotal role in constraining global warming and mitigating climate change. The landscape pattern of forests is being altered due to the combined effects of climate change and human interference. Furthermore, the relationship between forest pattern changes and carbon storage distribution in a long time series remains unclear. Therefore, it is necessary to examine the relationship between forest patterns and carbon density, investigating the variations and similarities in the changes in carbon density across different modes of pattern change over time, and suggestions for forest planning were provided from a perspective focused on pattern change to enhance carbon storage. The Google Earth Engine (GEE) platform's random forest model was used to map the spatial distribution of forests in Hunan Province for 1996 and 2020, followed by analyzing the correlation between the changes in forest patterns using the morphological spatial pattern analysis (MSPA) and carbon density simulated by the model. Results show that the net growth rate ((area in 2020-area in 1996)/area in 2020) of the forest in Hunan increased 26.76% between 1996 and 2020. The importance scores for the decade average temperature, short-wave length infrared band 1 (SWIR-1), and slope were the highest metrics in the model of carbon density, and were 0.127, 0.107 and 0.089, respectively. The vegetation carbon storage in Hunan Province increased by 31.02 Tg, from 545.91 Tg to 576.93 Tg in 25 years. This study demonstrates that vegetation carbon storage is influenced by the pattern type in both newly established and pre-existing forests ($p < 0.05$). The findings of this study offer empirical evidence to support forest management strategies targeted at enhancing carbon sequestration.

Keywords: global warming; vegetation carbon storage; Google Earth Engine (GEE); morphological spatial pattern analysis (MSPA); Hunan province

check for updates

Citation: Li, B.; Chen, L.; Wang, Q.; Wang, P. Analysis of Linkage between Long-Term Morphological Spatial Pattern Analysis and Vegetation Carbon Storage of Forests in Hunan, China. *Forests* **2024**, *15*, 428. https://doi.org/10.3390/f15030428

Academic Editor: Mark Vanderwel

Received: 24 January 2024
Revised: 17 February 2024
Accepted: 21 February 2024
Published: 23 February 2024

1. Introduction

Forest ecosystems offer a crucial service for limiting global warming and mitigating climate change. Global climate change is threatening the worldwide ecosystem due to human activities, and the rate of the temperature increase is faster than expected [1,2]. Meanwhile, the forest ecosystem plays an important role in preserving the existing carbon pool and increasing the carbon sink, which is considered to be critical to the restoration of global warming [3,4]. Therefore, the improvement of forest carbon stock is an important research topic regarding global climate change.

A nationwide effort is underway to improve the stock of forest carbon through afforestation and reforestation [5]. Specifically, the implementation of two policies—returning farmland to forest and vegetation protection—has led to an increase in the vegetation coverage and a reduction in the fragmentation within forest landscapes, which has caused landscape pattern changes in forests [6]. However, the long-term consequences of landscape change on carbon density and storage remain uncertain. Therefore, accurate estimates of the long-term carbon stocks of forest vegetation are critically important for effectively evaluating how landscape pattern change will influence forest carbon dynamics [7].

Forest vegetation carbon stocks can be estimated using three types of methods: the field-based method, satellite-based method, and process method [8]. Reliable information about the spatial distribution is fundamental for carbon stock. Field-based methods estimate forest carbon storage with field survey data, such as the stand age, diameter at breast height (DBH), and height of trees. The area-weighted average was applied when adapting the regional scale. Based on field surveys conducted from 2011 to 2015 in China, utilizing regional area data and the corresponding carbon storage weights, the estimated national forest carbon storage was determined to be 30.83 ± 1.57 Pg C [8]. However, field-based methods cannot track carbon sink dynamics promptly, nor can they grasp spatial heterogeneity within regions. Therefore, remote sensing images with wide coverage that are economical and timely are another option for carbon stock estimation [9]. The Moderate Resolution Imaging Spectroradiometer (MODIS), Sentinel series satellite and SPOT series satellite are some remote sensing data used for AGB estimation widely [10–12]. Landsat series satellites have become a standard tool for estimating biomass and carbon stocks due to their long time scales [13]. A study of the Amazon forest using Landsat imagery from 1984 to 2016 found that the carbon storage of degraded forests was 45.1% of that in intact forests [14]. A study of the forest carbon density in southern Iran using Landsat data from 1987 to 2015 demonstrated that the conservation and renewal of damaged forests is conducive to an increase in carbon density [15]. Therefore, how to use sampling data combined with Landsat series data to accurately evaluate long-term carbon storage changes needs to be further studied.

Numerous machine learning models have been widely used to develop remote sensing estimation models benchmarked with field survey data, including the support vector machine (SVM) [16,17], maximum entropy (MaxEnt) [18], artificial neural network (ANN) [19] and random forest (RF). Among them, random forest is an ensemble method used for classification and regression problems by building decision trees [20], and the good accuracy of RF has been well established [21]. However, previous work focused only on aboveground biomass, and a correlation between aboveground and subsurface carbon stocks of vegetation has been suggested.

Consequently, this analysis was conducted to examine the relationship between forest patterns and carbon density, investigating the variations and similarities in changes in carbon density across different modes of pattern change over time. Furthermore, suggestions for forest planning were provided from a perspective focused on pattern change with the aim of enhancing carbon storage. Therefore, based on the GEE platform and sample plot survey data, this study used a random forest model, Landsat series data, climate data, and topographic data to estimate the vegetation carbon storage in the forest ecosystem of Hunan province and its relationship with the landscape process, to provide theoretical support for afforestation and the conversion of farmland to forest to improve carbon storage.

2. Materials and Methods

2.1. Study Area

Hunan province is situated in the middle reaches of the Yangtze River, in central and southern China. Between the latitudes 24°38′–30°08′ N and longitudes 108°47′–114°15′ E, Hunan has a total area of 21.18×10^4 km^2, and accounts for 2.2% of China's land area (Figure 1). The GDP of Hunan increased from 355.149 billion yuan in 2000 to 3642.578 billion yuan in 2018, while the per capita GDP increased from 5425 yuan in 2000 to 52.949 yuan in 2018 [22].

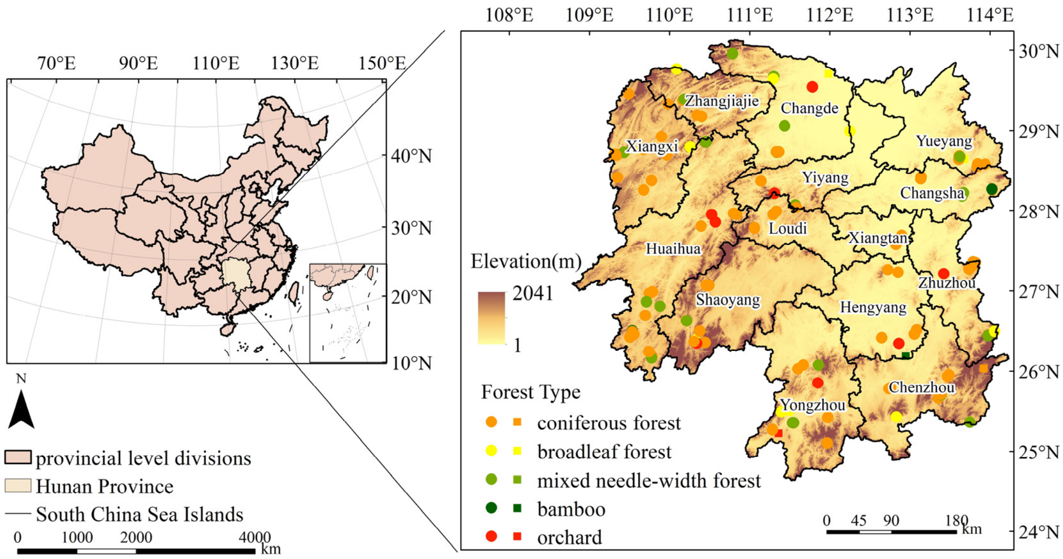

Figure 1. The spatial location map of the research area in China and sampling points, including the training set (circle) and the verification set (square).

With a subtropical monsoon climate, the average annual precipitation of the study area is 1200–1700 mm, and the mean annual temperature is 16–18 °C. Under this climate condition, the vegetation in Hunan is mainly evergreen broad-leaved forest, deciduous broad-leaved forest, coniferous forest, and bamboo forest, with rich tree species resources and high forest coverage. In 2021, Hunan Province had 11.91×10^4 km^2 of forest, accounting for 59.97 percent of the administrative area, according to statistics from the Hunan Forestry Bureau.

2.2. Land Use Classification of 1996–2020 in Hunan Province

2.2.1. Training and Validation Sample Selection

Land-use types were categorized into two primary classes (forest and non-forest). A minimum of 600 training samples for each class were chosen with the aid of high-resolution imagery from Google Earth and fieldwork [23]. The precipitation, tree height, and leaf area index were used as supporting information for selecting the training samples to improve the classification accuracy. As a result, 70% of the polygons were used for training the models, and 30% were used for assessing the accuracy of the models.

2.2.2. Satellite Data Sources and Processing

In Hunan province, Landsat images from 1996 to 2020 were used for land use mapping. The images were derived from the Landsat 5 TM (1996) and Landsat 8 OLI/TIRS satellites (2020) with 30 m × 30 m resolution, cloud removal was used for all images. All images were chosen and processed on the Google Earth Engine (GEE) directly, which is a computing platform that allows users to run a geospatial analysis on Google's infrastructure [24].

2.2.3. Land-Use Mapping in Hunan

The land-use classification mapping in Hunan was performed with a random forest machine learning classifier, also using the GEE platform. Random forest is an ensemble learning algorithm designed to perform classification using an ensemble of decision trees, each consisting of a randomly chosen set. Since each tree returns a decision, class probabilities were estimated from the votes [20].

In the GEE, the land use classification by random forest was achieved by invoking the ee.smileRandomForest function, which required the setting of three parameters: the number of decision trees to create, the number of variables per split, and the randomization seed. Among the parameters, the first two parameters were used to improve the fitting accuracy, another parameter was used to ensure model reproducibility.

2.2.4. Evaluation of Land-Use Classification Accuracy

The kappa coefficient as shown in Equation (1) was used to verify and evaluate whether there was a consistency between the predicted and actual results, to test the accuracy of the classification.

$$K = \frac{N\sum_{k=1}^{n} Pkk - \sum_{k=1}^{n}\left(\sum_{i=1}^{n} p_{ki}\sum_{j=1}^{n} p_{kj}\right)}{N^2 - \sum_{k=1}^{n}\left(\sum_{i=1}^{n} P_{ki}\sum_{j=1}^{n} p_{kj}\right)} \quad (1)$$

The symbol K represents the kappa coefficient, while n denotes the total number of categories. Pkk refers to the number of correct classifications for the k-th sample in the confusion matrix, $\sum_{i=1}^{n} P_{ki}$ and $\sum_{j=1}^{n} p_{kj}$ represent the sample size on columns i and j, respectively. N indicates the total number of samples used for accuracy evaluation.

2.3. Changes in Spatial Patterns of Forest between 1996 and 2020

A morphological spatial pattern analysis (MSPA) method was employed to examine the changes in forest patterns across Hunan province from 1996 to 2020. The pattern classes were identified into seven distinct types by MSPA: core, islet, perforation, edge, loop, bridge, and branch. The core pixels were defined as foreground pixels that have a greater distance to the background than the given size parameters. Islet pixels refer to connected components in the foreground that do not contain any core pixel. Bridge pixels are connector pixels originating from two or more core connected components. Boundary pixels are unclassified foreground pixels whose distance to the core pixels is lower than or equal to the given size parameters, outer boundaries as edges and inner boundaries as perforations. Loop pixels are connector pixels emanating from the same core connected component. The remaining pixels were classified as branches [25]. The MSPA was implemented utilizing the GuidosToolbox v3.0 (ISPRA, Rome, Italy) [26], employed with the forest as the foreground, while the non-forest served as the background. The MSPA was conducted with a 30 m width of edge and eight neighbor connectivity [27].

2.4. Estimation of Forest Carbon Stocks between 1996 and 2020

2.4.1. Field Survey Data

To obtain the measured value of carbon stock required for establishing the model, 108 and 119 field survey plots were established in 2011 and 2012, respectively. The plots were evenly distributed across the spatial extent of Hunan Province (Figure 1), consisting of broadleaf forest (18), coniferous forest (149), mixed needle-width forest (42), bamboo forest (6), and orchard (12). The height and DBH of each tree in each quadrat were measured, and the root systems were dug up at the same time. As for the shrubs, three random 2 m $\times$ 2 m plots were placed at each site to harvest and weigh them, and a 1 m^2 plot was laid in them for collecting the herb and leaf litter layer [28].

The total biomass was calculated as the sum of the tree biomass, shrub biomass, herb biomass and leaf litter biomass. The tree biomass, including the leaf biomass, stem biomass, and root biomass, was calculated from the tree height and DBH using published growth equations. The shrub, herb biomass, and leaf litter biomass were directly expressed as their dry weights [28].

The carbon stock was obtained by multiplying the aboveground biomass by the carbon conversion coefficients [29], which were calculated based on the measured data, and converted to density to build a carbon density model. The models were trained using 90% of the sample plots, while the remaining 10% were used to assess the accuracy of the model.

2.4.2. Variable Extraction of Carbon Storage Estimation Model

The predictor variables were classified into four categories for the spatial prediction of carbon density [11,12]: single-band reflectance, topographic variables, vegetation indices, and climate variables. In order to ensure robust model construction, we incorporated a wide range of observed variables into these four categories for multiple testing. The final model consists of the 15 variables below which have been selected based on their highest contribution and accuracy. Detailed information regarding these predictor variables can be found in Table 1.

Table 1. Details of Predictor Variables in Model of Carbon Density.

Variables	Formula
Single band reflectance	Blue (0.45–0.52 µm)
	Green (0.52–0.60 µm)
	Red (0.63–0.69 µm)
	Near infrared band (NIR, 0.76–0.90 µm)
	Short-wave length infrared band 1 (SWIR 1, 1.55–1.75 µm)
	Short-wave length infrared band 2 (SWIR 2, 2.08–2.35 µm)
Topographic variable	Slope
Vegetation indices	Normalized difference vegetation index (NDVI) = (NIR − Red)/(NIR + Red)
	Differenced vegetation index (DVI) = NIR − Red
	Ratio Vegetation Index (RVI) = Red/NIR
	Blue Normalized difference vegetation index (BNDVI) = (NIR − Blue)/(NIR + Blue)
Climate variable	Annual minimum temperature (TMIN)
	Total annual precipitation (TAP)
	Annual maximum temperature (TMAX)
	Decade mean of annual temperature (DMAT)

Single-band reflectance and vegetation variables were derived from the Landsat 5 TM (1996), Landsat 7 ETM + (2011–2012), and Landsat 8 OLI/TIRS satellites (2020) with 30 m × 30 m resolution, gap fill was used for Landsat 7 only. Climate variables were obtained from the China Meteorological Data Service Centre (http://data.cma.cn/en). The topographic variable was obtained from digital elevation data of the Shuttle Radar Topography Mission (SRTM) [30].

2.4.3. Simulation and Verification of Vegetation Carbon Density in Hunan Province

The vegetation carbon density mapping in Hunan was performed with random forest in the GEE platform. Finally, 50 trees and 11 variables were selected for RF classification by performing multiple fits. The coefficient of determination (R^2) was used for model evaluation as shown in Equation (2). Ultimately, the spatial distribution of vegetation carbon density in Hunan Province in 1996 and 2020 was estimated using the random forest model's regression function in GEE.

$$R^2 = 1 - \sum_{i=1}^{n}(C_i - \hat{C}_i)^2 / \sum_{i=1}^{n}(C_i - \overline{C})^2 \quad (2)$$

where C_i are observed values, $\hat{C}i$ are estimated values, $\overline{C}$ is the average of the observed values, and n is the number of samples.

2.5. Relationship between Forest Pattern and Carbon Density

A one-way ANOVA was employed to investigate the association between the change in forest patterns and carbon densities in 2020. A transition matrix was utilized to detect changes in forest pattern types between 1996 and 2020, which were categorized into two groups: forty-nine pre-existing forest types (forests present in both 1996 and 2020) and seven newly added forest types (areas that were non-forest in 1996 but became forested by

2020). A total of 10,000 spatially balanced points were randomly generated in each type, to analyze the association between different forest patterns and carbon densities in 2020. Due to the non-homogeneity of variance, the Kruskal–Wallis test for intra-group differences was applied, followed by multiple comparisons using the Nemenyi test, implemented by packages PMCMRplus in R 4.1.2.

3. Results

3.1. Accuracy Assessment of Land Use

A confusion matrix between the validation data and the classification result was calculated. In 1996 and 2020, the overall accuracy (OA) of the classification result was greater than 90%, and the producer's accuracy (PA) and user's accuracy (UA) of the forest were all exceeding 80% (Table 2). The results indicated the precision and dependability of the classification results.

Table 2. Forest classification accuracy of Hunan Province in 1996 and 2020.

Year	Kappa	Producer's Accuracy	User's Accuracy	Overall Accuracy
1996	0.79	87.6%	80.92%	91.77%
2020	0.80	86.7%	85.34%	91.82%

3.2. Evolution of Hunan's Forest Spatial Patterns

The statistical result of the forest spatial distribution in Hunan Province in 1996 and 2020 (Figure 2) shows that the net growth rate of the forest in Hunan increased 26.76% between 1996 and 2020, from 8.25×10^4 km^2 to 11.27×10^4 km^2.

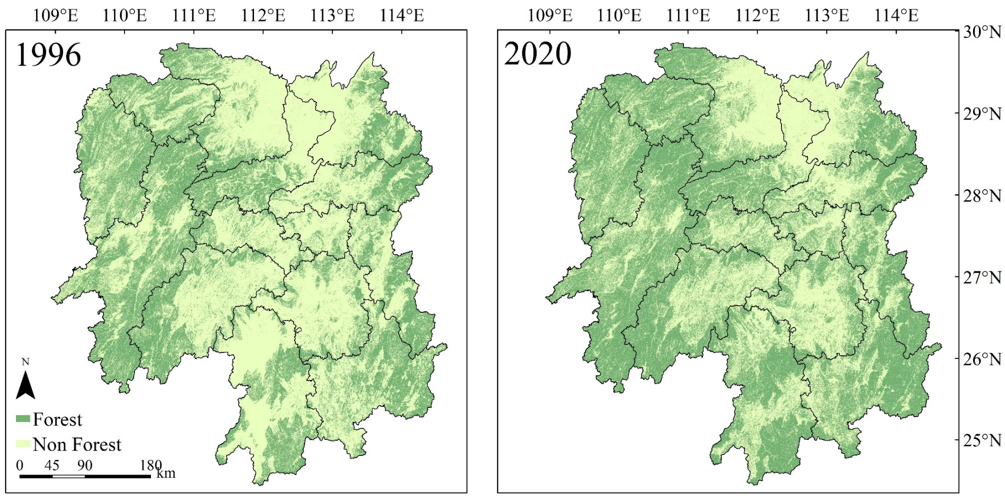

Figure 2. Forest spatial distribution of Hunan in 1996 and 2020.

In 2020, the four cities with the largest forest area in Hunan Province were Huaihua (1.88×10^4 km^2), Yongzhou (1.27×10^4 km^2), Chenzhou (1.24×10^4 km^2), and Shaoyang (1.13×10^4 km^2), concentrated in the west, south, and southwest of Hunan Province (Figure 3). The forest areas of cities in Hunan were also counted at various times. The results showed that the forest areas of all cities in Hunan increased between 1996 and 2020. Of those, the city with the most forest growth was Huaihua (4.99×10^3 km^2), located in the southwest of the province. Followed by Yongzhou (4.04×10^3 km^2), which is in the southern region. Similarly, the cities with the highest proportion of newly added forests were Chenzhou and Yongzhou, which were 22.98% and 18.9%, respectively.

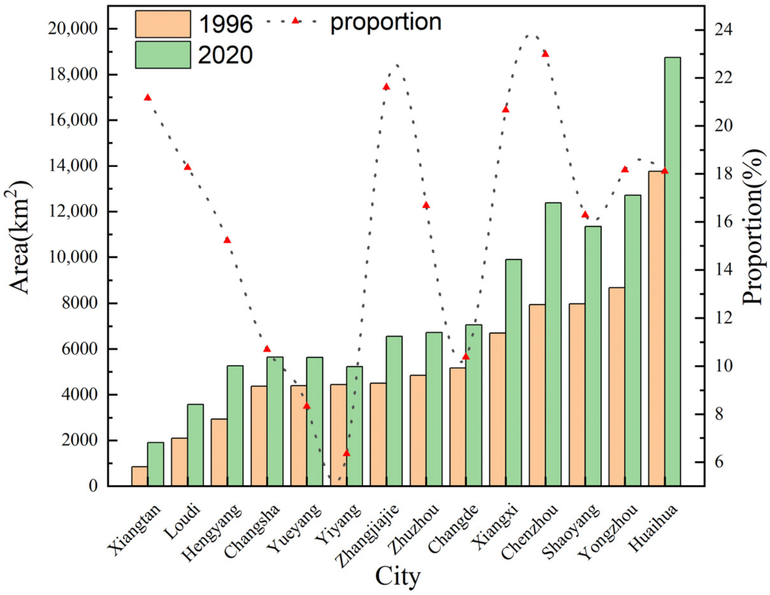

Figure 3. Forest areas in cities of Hunan in 1996 (green pillar) and 2020 (orange pillar) and proportion of newly added forest in the area of the urban administrative region (line chart).

The seven forest landscape types of Hunan province in 1996 and 2020 were obtained based on the classification of forest patch types from the MSPA method (Figure 4). The number of different morphological types showed that the proportion of the core area increased from 21.9% in 1996 to 34.17% in 2020, increased by 25,893.58 km^2 for 25 years. The change in islet pixels was extremely low for Hunan, from 1.83% in 1996 to 1.66% in 2020. For the three connectors, including the bridge, loop, and branch, the percentage was very small. The increases in the edge area, loop, and branch were simultaneous with the increase in the core area. On the contrary, the bridge decreased by 1330.53 km^2.

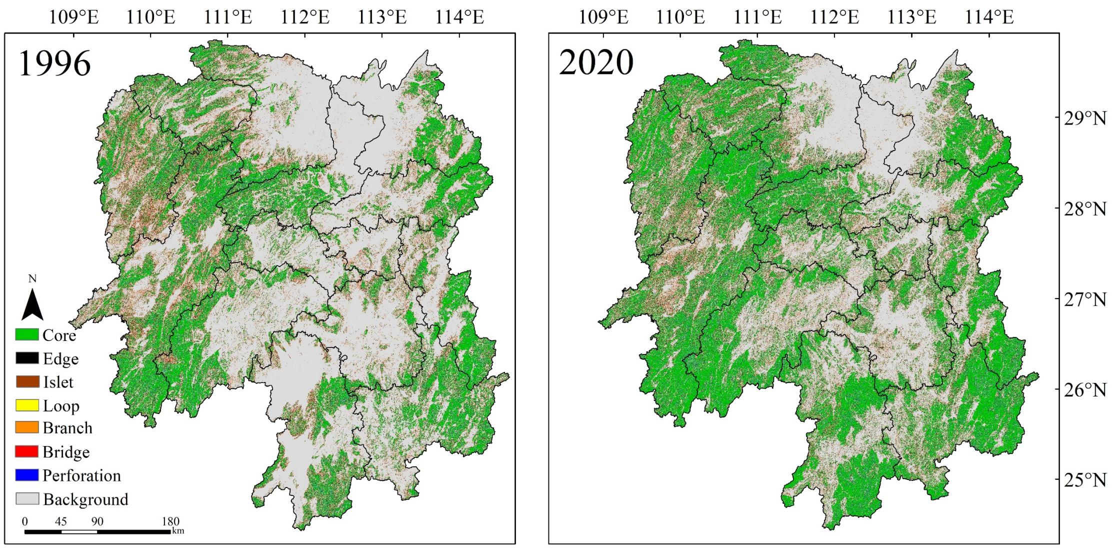

Figure 4. Forest landscape types of Hunan province in 1996 and 2020.

The areas transferred between different types were obtained from the transfer matrix (Figure 5). The primary type core in 1996, except 79.65% that remained unchanged, was mainly converted to background (7.30%) by 2020, followed by the edge (4.68%) and loop (4.31%). For the core in 2020, the transformation mainly occurred in the background, accounting for 24.50% of the core area of 2020, followed by the bridge (4.72%) and perforation (3.83%).

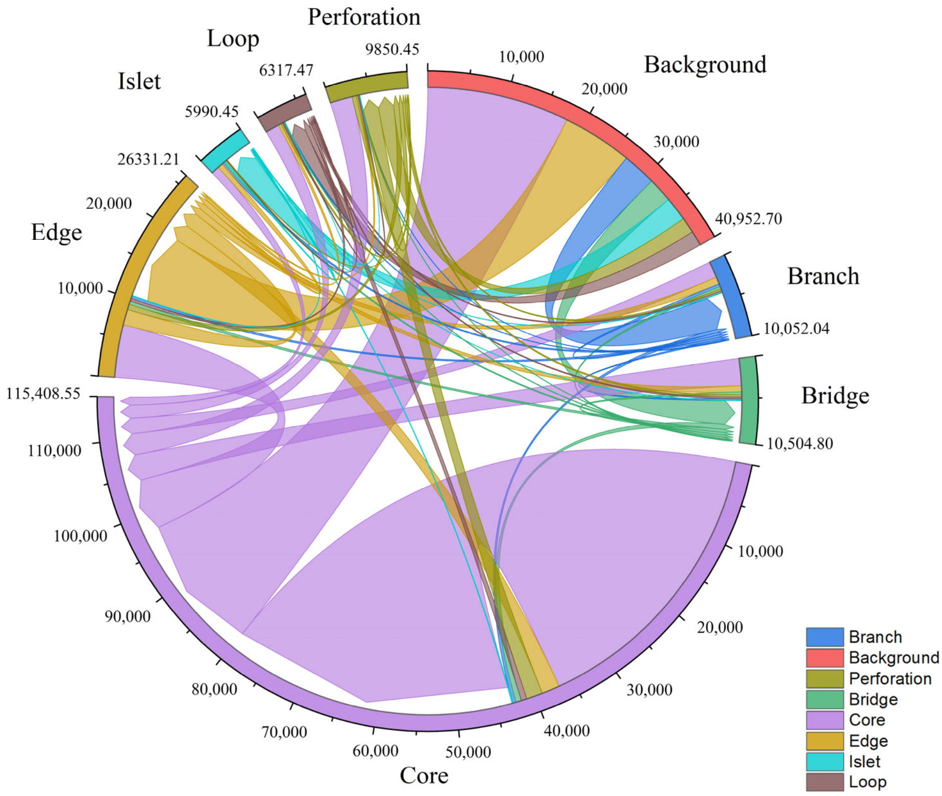

Figure 5. Chord diagram of transfers area(km^2) between different pattern types from 1996 to 2020.

3.3. Spatial Distribution of Carbon Density in Hunan Province

3.3.1. Random Forest Modeling for Carbon Density

The spatial distribution analysis of the actual carbon density plots at the test sites reveal that the average carbon density of the test sites was 4.83 kg/m^2. At the same time, the minimum carbon density recorded was 0.48 kg/m^2, observed in a coniferous plot situated in the northeastern region of Hunan Province, while the maximum value reached 12.128 kg/m^2, observed in a mixed forest plot located in the southeastern part of the research area. Through the comparison of the actual carbon density values and calibration data of modeling using formula 2, the random forest regression model used to estimate the forest carbon density generated by the GEE platform was accurate with a 0.73. Therefore, the values of carbon density estimated from the random forest model could be suitable for estimating carbon density and carbon storage in Hunan province.

The final random forest regression model generated by the GEE contained 15 variables. All importance scores of variables were normalized (Figure 6). From the result of the importance score, the BNDVI, and DVI were the most helpful vegetation indices for the carbon storage of forests in Hunan. As for spectral bands, the two most contributing bands were the SWIR1 and SWIR2. Among the climatic factors, the decade mean of annual temperature (DMAT) and total annual precipitation (TAP) were the most significant variables. In general, the importance scores for the DMAT, SWIR 1, slope, and TAP were the highest metrics, the least were the annual minimum temperature (TMIN), annual maximum temperature (TMAX), blue band, and green band.

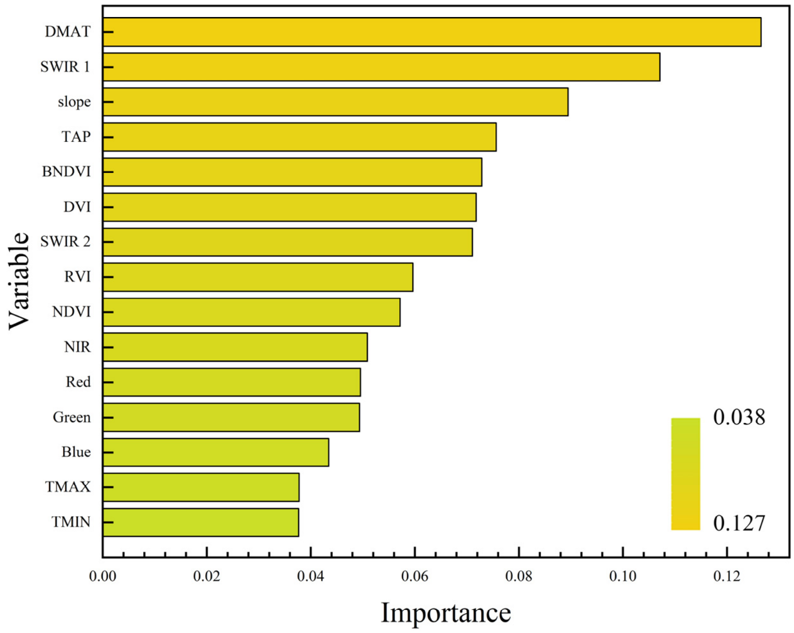

Figure 6. Importance score of variables in the random forest modeling for carbon density. Note: DMAT: decade mean of annual temperature, SWIR 1: short-wave length infrared band 1, TAP: total annual precipitation, BNDVI: blue normalized difference vegetation index, DVI: difference vegetation index SWIR 1: short-wave length infrared band 2, RVI: ratio vegetation index, NDVI: normalized difference vegetation index, NIR: near infrared band, TMAX: annual maximum temperature, TMIN: annual minimum temperature.

3.3.2. Spatial Distribution of Carbon Density

The spatial carbon density in Hunan between 1996 and 2020 was estimated from the random forest in the GEE platform (Figure 7). In 1996, the maximum and minimum ranged from 1.78 kg/m^2 to 11.15 kg/m^2 with a mean carbon density of 6.94 kg/m^2. As of 2020, the carbon density ranged from 4.04 kg/m^2 to 7.80 kg/m^2, with a mean density of 5.12 kg/m^2.

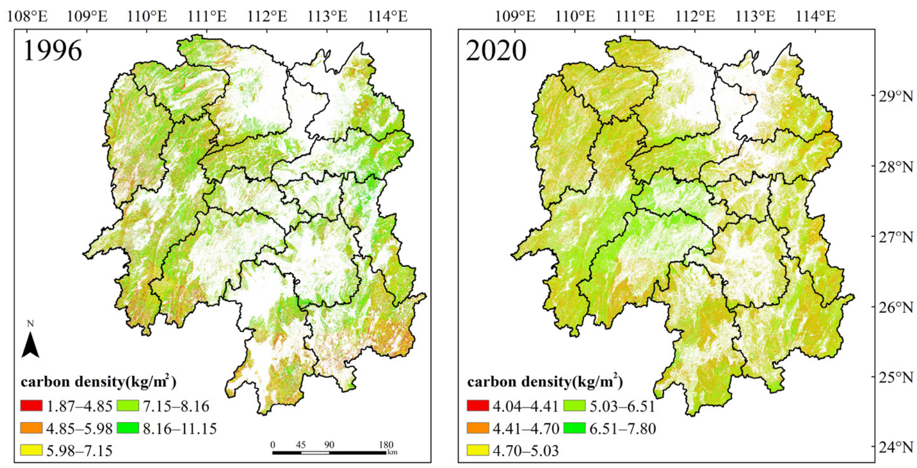

Figure 7. Carbon density spatial distribution of Hunan in 1996 and 2020.

After converting to carbon storage, the vegetation carbon storage in Hunan Province increased by 31.02 Tg, from 545.91 Tg to 576.93 Tg in 25 years.

3.4. Relationship between Forest Pattern and Carbon Density

The carbon density corresponding to the MSPA type of forest was obtained and a one-way analysis of variance was performed. The results show that the carbon density in the islet area was significantly higher than that in other types of areas (Figure 8a), followed by pixels of the edge, branch, and core. In contrast, the carbon density of the perforation was significantly lower than that of all other types. In addition, there was no significant difference between the carbon density of the loop and bridge pixels.

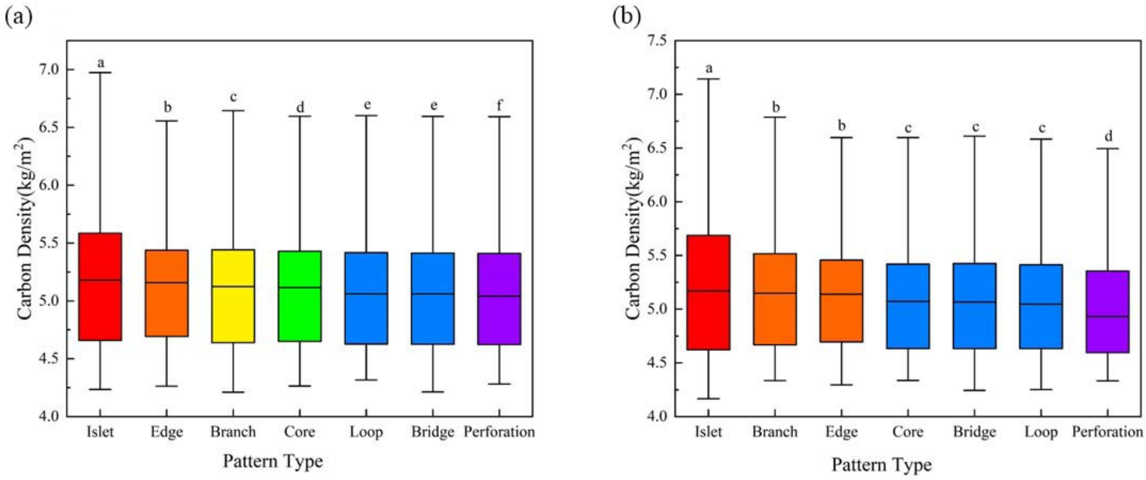

Figure 8. Relationship between carbon density and pattern type following the conversion from forest to forest (**a**) and the conversion from non-forest to forest (**b**). Significant differences ($p < 0.05$) are indicated by different lowercase letters.

The relationship between the carbon density and pattern type following the conversion from non-forest to forest was also examined for the period spanning 1996 to 2020 (Figure 8b). The findings revealed significant variations in carbon density among different forest types ($p < 0.05$). Specifically, the islet and perforation exhibited significantly higher and lower carbon densities, respectively, compared to other forest types within the newly established forest area. Meanwhile, the differences between the branch and edge, as well as between the core, bridge, and loop were not statistically significant.

4. Discussion

4.1. The Platform of the Google Earth Engine

The land use classification and carbon density modeling in Hunan Province between 1996 and 2020 were performed in a random forest model, based on the remote sensing platform of the Google Earth Engine (GEE), promptly and precisely. According to the fieldwork and Google high-resolution imagery, the overall accuracy of the forest type exceeded 80%, indicating that the results of the forest spatial distribution in Hunan were accurate and reliable (Table 2). Simultaneously, the carbon density model was also more accurate than 0.7, showing that the model was capable of estimating the spatial distribution of the forest carbon density in Hunan Province. Therefore, the integration of the random forest algorithm and GEE platform can effectively facilitate the analysis of the spatial distribution and carbon density changes in forests. We considered orchards in the research object, considering that orchards are also trees with a carbon sequestration function. Moreover, in the primary classification of land use, the machine learning model was more likely to identify orchards as forests than farmland. For the accuracy of the carbon storage mode, we regard orchards as an agroforestry system.

The GEE is a free and cloud-based computing platform, which allows data browsing and processing online [31]. Besides, the data catalog of the GEE encompasses not only remote sensing satellites, but also includes climate and weather datasets and geophysical datasets [24]. However, the meteorological data available for this study were primarily global in scale and exceed our requirements [32]. Therefore, we opted for an offline–online hybrid approach whereby the data was processed using QGIS v3.8 (Eastern Cape, South Africa). before being uploaded to the GEE platform for analysis.

Random forest, a nonparametric ensemble modeling approach that is resistant to overfitting, constructs multiple small regression trees that contribute to predictions, insensitivity to noisy data in training datasets, and is capable of handling noise and large datasets [20,33]. The random forest algorithm has become a widely adopted approach for estimating carbon stocks, and has been seamlessly integrated into the GEE platform.

4.2. The Factors of the Forest Carbon Density Model

Our results indicate that climatic factors play a role in estimating the carbon stock of forests in Hunan (Figure 6). The spatial pattern of the carbon density is strongly correlated with climate variables and has been well established [34]. Temperature is frequently linked to plant metabolism, which in turn affects growth and respiration rates, ultimately impacting forest productivity and carbon storage [35]. Meanwhile, precipitation has been shown to be remarkably well correlated with carbon density [36]. The slope is an important factor that affects plant growth and development, because the variation in slopes has an impact on the angle of incidence and reflectivity of solar radiation [37,38].

The order of importance of the original bands in the model varies with the forest structure [39]. The short-wave infrared 1 (SWIR1) band is the most important of all the original bands in this study. In a Brazilian study, the fit degree of the biomass model involved in the SWIR band was the highest [40]. The red and near-infrared bands, despite their low importance in the model, were the main bands of the vegetation index (Figure 6).

The normalized difference vegetation index (NDVI) [41] is the most widely used vegetation index, which has a sensitive response to green vegetation and vegetation change [42]. The blue normalized difference vegetation index (BNDVI), modified based on the NDVI with different visible spectra, is determined by the concentration of chlorophyll [43,44]. The ratio vegetation index (RVI) is based on the principle that red light is preferentially absorbed by leaves compared with infrared light [45]. The difference vegetation index (DVI) is capable of distinguishing vegetation from soil background information [46].

4.3. Forest Pattern and Carbon Density in Hunan Province

The MSPA has been widely used for various purposes such as mapping spatial patterns, landscape connectivity, and indicating forest ecosystem quality. The results of a morphological spatial pattern analysis (MSPA) provide spatially explicit information regarding the pattern and composition of landscapes, in contrast to the conventional fragmentation analyses [47,48]. The analysis results of the MSPA (Figure 4) showed that the proportion of core in the research area had witnessed a steady increase (21.94% in 1996 to 34.17% in 2020), suggesting a reduction in forest landscape fragmentation levels in Hunan [49]. Simultaneously, the perforation and edge are boundary pixels, situated at a certain distance from the core pixels. The proportion of perforation and edge also exhibited an upward trend throughout the study, which may suggest an increase in the initiation of forest landscapes [50]. On the contrary, the islet proportion had experienced a decline (1.83% in 1996 to 1.66% in 2020) and may face encroachment due to urban expansion [51]. The pixels associated with the core pixels are called junctions and include loops, bridges, and branches. Of these, the proportion of bridges, which serve as connectors linking different core areas, had decreased while the proportions of the remaining two types had increased, suggesting that although the core area of Hunan Province had expanded, urban development would be likely impeding connectivity between forest patches.

The forest's carbon sequestration function is closely linked to temporal changes in landscape patterns. The investigation of the interplay among landscape configurations, processes, and ecological functions has always been a fundamental issue in the fields of landscape ecology and forest management [50]. This study demonstrates that vegetation carbon storage is influenced by the pattern type in both newly established and pre-existing forests (Figure 8a,b). Due to the forest margin effect and the forest window effect, the carbon density of pattern types at the outer forest margin surpasses that of both the core area and inner forest margin. The forest edges typically exhibit a greater abundance of pioneer and xeric plant species compared to the interior, along with higher densities of shrubs and herbaceous ground layer vegetation extending several meters into the forest, as well as a higher level of species richness than the interior. However, vegetation in marginal areas is more vulnerable to wind and human activity, so it is also necessary to protect or restore large core areas [52]. These findings provide valuable data for informing afforestation and reforestation planning.

5. Conclusions

This study examined the relationship between changes in forest landscape patterns and carbon density or carbon storage over a long time series. The random forest model in the GEE platform and an MSPA method were employed to assess alterations in the spatial distribution and patterns of forests in Hunan Province between 1996 and 2020. Over 25 years, the forest area in Hunan Province increased from 8.25×10^4 km^2 to 11.27×10^4 km^2, with an expansion observed in core areas while isolated island areas decreased. By integrating point data, remote sensing data, climate data, and terrain data through a regression algorithm within the random forest model on the GEE platform, we obtained a vegetation carbon density model for Hunan Province. Furthermore, we estimated vegetation carbon storage for both 1996 and 2020. The variance analysis of vegetation density across different forest pattern types revealed significant differences in carbon density. We expect the findings of this study to offer empirical evidence to support forest management strategies targeted at enhancing carbon sequestration.

Author Contributions: Conceptualization, Q.W.; data curation, L.C.; formal analysis, B.L.; funding acquisition, Q.W.; investigation, L.C.; methodology, B.L.; software, B.L.; supervision, P.W.; writing—original draft, B.L.; writing—review and editing, L.C. and Q.W. All authors have read and agreed to the published version of the manuscript.

Funding: This research was funded by the National Natural Science Foundation of China, grant numbers 32171752 and 31830015, and the Natural Science Foundation of Hunan Province, grant number 2022JJ30468, and the National Sustainable Development Agenda Construction Program of Chenzhou Innovation Demonstration Area, grant number 2021sfq19–1.

Data Availability Statement: The data that support the findings of this study are available from the corresponding author on request.

Conflicts of Interest: The authors declare that they have no competing financial interests or personal relationships that are relevant to the content of this article.

References

1. Friedlingstein, P.; O'Sullivan, M.; Jones, M.W.; Andrew, R.M.; Hauck, J.; Olsen, A.; Peters, G.P.; Peters, W.; Pongratz, J.; Sitch, S.; et al. Global Carbon Budget 2020. *Earth Syst. Sci. Data* **2020**, *12*, 3269–3340. [CrossRef]
2. Tollefson, J. Climate change is hitting the planet faster than scientists originally thought. *Nature* **2022**. [CrossRef]
3. Pan, Y.D.; Birdsey, R.A.; Fang, J.Y.; Houghton, R.; Kauppi, P.E.; Kurz, W.A.; Phillips, O.L.; Shvidenko, A.; Lewis, S.L.; Canadell, J.G.; et al. A Large and Persistent Carbon Sink in the World's Forests. *Science* **2011**, *333*, 988–993. [CrossRef]
4. Griscom, B.W.; Adams, J.; Ellis, P.W.; Houghton, R.A.; Lomax, G.; Miteva, D.A.; Schlesinger, W.H.; Shoch, D.; Siikamaki, J.V.; Smith, P.; et al. Natural climate solutions. *Proc. Natl. Acad. Sci. USA* **2017**, *114*, 11645–11650. [CrossRef]
5. Jia, X.; Zha, T.S.; Wu, B.; Zhang, Y.Q.; Chen, W.J.; Wang, X.P.; Yu, H.Q.; He, G.M. Temperature Response of Soil Respiration in a Chinese Pine Plantation: Hysteresis and Seasonal vs. Diel Q(10). *PLoS ONE* **2013**, *8*, e57858. [CrossRef]
6. Walz, U. Monitoring of landscape change and functions in Saxony (Eastern Germany)—Methods and indicators. *Ecol. Indic.* **2008**, *8*, 807–817. [CrossRef]
7. Li, X.Y.; Guo, J.M.; Qi, S.Z. Forestland landscape change induced spatiotemporal dynamics of subtropical urban forest ecosystem services value in forested region of China: A case of Hangzhou city. *Environ. Res.* **2021**, *193*, 110618. [CrossRef]
8. Sun, W.L.; Liu, X.H. Review on carbon storage estimation of forest ecosystem and applications in China. *For. Ecosyst.* **2019**, *7*, 4. [CrossRef]
9. Kumar, L.; Mutanga, O. Remote Sensing of Above-Ground Biomass. *Remote Sens.* **2017**, *9*, 935. [CrossRef]
10. Li, W.; Niu, Z.; Liang, X.L.; Li, Z.Y.; Huang, N.; Gao, S.; Wang, C.; Muhammad, S. Geostatistical modeling using LiDAR-derived prior knowledge with SPOT-6 data to estimate temperate forest canopy cover and above-ground biomass via stratified random sampling. *Int. J. Appl. Earth Obs.* **2015**, *41*, 88–98. [CrossRef]

11. Wai, P.; Su, H.Y.; Li, M.S. Estimating Aboveground Biomass of Two Different Forest Types in Myanmar from Sentinel-2 Data with Machine Learning and Geostatistical Algorithms. *Remote Sens.* **2022**, *14*, 2146. [CrossRef]
12. Yin, G.D.; Zhang, Y.; Sun, Y.; Wang, T.; Zeng, Z.Z.; Piao, S.L. MODIS Based Estimation of Forest Aboveground Biomass in China. *PLoS ONE* **2015**, *10*, e0130143. [CrossRef]
13. Zhu, X.L.; Liu, D.S. Improving forest aboveground biomass estimation using seasonal Landsat NDVI time-series. *ISPRS J. Photogramm. Remote Sens.* **2015**, *102*, 222–231. [CrossRef]
14. Rappaport, D.I.; Morton, D.C.; Longo, M.; Keller, M.; Dubayah, R.; dos-Santos, M.N. Quantifying long-term changes in carbon stocks and forest structure from Amazon forest degradation. *Environ. Res. Lett.* **2018**, *13*, 065013. [CrossRef]
15. Safari, A.; Sohrabi, H. Effect of climate change and local management on aboveground carbon dynamics (1987-2015) in Zagros oak forests using Landsat time-series imagery. *Appl. Geogr.* **2019**, *110*, 102048. [CrossRef]
16. Deb, D.; Deb, S.; Chakraborty, D.; Singh, J.P.; Singh, A.K.; Dutta, P.; Choudhury, A. Aboveground biomass estimation of an agro-pastoral ecology in semi-arid Bundelkhand region of India from Landsat data: A comparison of support vector machine and traditional regression models. *Geocarto Int.* **2022**, *37*, 1043–1058. [CrossRef]
17. Mountrakis, G.; Im, J.; Ogole, C. Support vector machines in remote sensing: A review. *ISPRS J. Photogramm. Remote Sens.* **2011**, *66*, 247–259. [CrossRef]
18. Rodriguez-Veiga, P.; Saatchi, S.; Tansey, K.; Balzter, H. Magnitude, spatial distribution and uncertainty of forest biomass stocks in Mexico. *Remote Sens. Environ.* **2016**, *183*, 265–281. [CrossRef]
19. Nandy, S.; Singh, R.; Ghosh, S.; Watham, T.; Kushwaha, S.P.S.; Kumar, A.S.; Dadhwal, V.K. Neural network-based modelling for forest biomass assessment. *Carbon Manag.* **2017**, *8*, 305–317. [CrossRef]
20. Breiman, L. Random forests. *Mach. Learn.* **2001**, *45*, 5–32. [CrossRef]
21. Han, L.; Yang, G.J.; Dai, H.Y.; Xu, B.; Yang, H.; Feng, H.K.; Li, Z.H.; Yang, X.D. Modeling maize above-ground biomass based on machine learning approaches using UAV remote-sensing data. *Plant Methods* **2019**, *15*, 10. [CrossRef]
22. Chen, W.X.; Zhou, T.; Liang, J.L. Urbanization, ecosystem services, and their interactive coercive relationship in Hunan Province, China. *Environ. Sci. Pollut. Res.* **2023**, *30*, 3416–3431. [CrossRef] [PubMed]
23. Yin, H.; Khamzina, A.; Pflugmacher, D.; Martius, C. Forest cover mapping in post-Soviet Central Asia using multi-resolution remote sensing imagery. *Sci. Rep.* **2017**, *7*, 1375. [CrossRef] [PubMed]
24. Gorelick, N.; Hancher, M.; Dixon, M.; Ilyushchenko, S.; Thau, D.; Moore, R. Google Earth Engine: Planetary-scale geospatial analysis for everyone. *Remote Sens. Environ.* **2017**, *202*, 18–27. [CrossRef]
25. Soille, P.; Vogt, P. Morphological segmentation of binary patterns. *Pattern Recognit. Lett.* **2009**, *30*, 456–459. [CrossRef]
26. Vogt, P.; Riitters, K. GuidosToolbox: Universal digital image object analysis. *Eur. J. Remote Sens.* **2017**, *50*, 352–361. [CrossRef]
27. Ostapowicz, K.; Vogt, P.; Riitters, K.H.; Kozak, J.; Estreguil, C. Impact of scale on morphological spatial pattern of forest. *Landsc. Ecol.* **2008**, *23*, 1107–1117. [CrossRef]
28. Chen, L.C.; Guan, X.; Li, H.M.; Wang, Q.K.; Zhang, W.D.; Yang, Q.P.; Wang, S.L. Spatiotemporal patterns of carbon storage in forest ecosystems in Hunan Province, China. *Forest Ecol. Manag.* **2019**, *432*, 656–666. [CrossRef]
29. Torres, C.; Jacovine, L.A.G.; de Olivera Neto, S.N.; Fraisse, C.W.; Soares, C.P.B.; de Castro Neto, F.; Ferreira, L.R.; Zanuncio, J.C.; Lemes, P.G. Greenhouse gas emissions and carbon sequestration by agroforestry systems in southeastern Brazil. *Sci. Rep.* **2017**, *7*, 16738. [CrossRef]
30. Farr, T.G.; Rosen, P.A.; Caro, E.; Crippen, R.; Duren, R.; Hensley, S.; Kobrick, M.; Paller, M.; Rodriguez, E.; Roth, L.; et al. The shuttle radar topography mission. *Rev. Geophys.* **2007**, *45*, RG2004. [CrossRef]
31. Zhao, Q.; Yu, L.; Li, X.C.; Peng, D.L.; Zhang, Y.G.; Gong, P. Progress and Trends in the Application of Google Earth and Google Earth Engine. *Remote Sens.* **2021**, *13*, 3778. [CrossRef]
32. Khan, R.; Gilani, H. Global drought monitoring with big geospatial datasets using Google Earth Engine. *Environ. Sci. Pollut. Res.* **2021**, *28*, 17244–17264. [CrossRef]
33. Rodriguez-Galiano, V.F.; Ghimire, B.; Rogan, J.; Chica-Olmo, M.; Rigol-Sanchez, J.P. An assessment of the effectiveness of a random forest classifier for land-cover classification. *ISPRS J. Photogramm. Remote Sens.* **2012**, *67*, 93–104. [CrossRef]
34. Tang, X.L.; Zhao, X.; Bai, Y.F.; Tang, Z.Y.; Wang, W.T.; Zhao, Y.C.; Wan, H.W.; Xie, Z.Q.; Shi, X.Z.; Wu, B.F.; et al. Carbon pools in China's terrestrial ecosystems: New estimates based on an intensive field survey. *Proc. Natl. Acad. Sci. USA* **2018**, *115*, 4021–4026. [CrossRef] [PubMed]
35. Cooper, L.A.; Ballantyne, A.P.; Holden, Z.A.; Landguth, E.L. Disturbance impacts on land surface temperature and gross primary productivity in the western United States. *J. Geophys. Res.-Biogeosci.* **2017**, *122*, 930–946. [CrossRef]
36. Becknell, J.M.; Kucek, L.K.; Powers, J.S. Aboveground biomass in mature and secondary seasonally dry tropical forests: A literature review and global synthesis. *Forest Ecol. Manag.* **2012**, *276*, 88–95. [CrossRef]
37. Lang, A.C.; Hardtle, W.; Bruelheide, H.; Geissler, C.; Nadrowski, K.; Schuldt, A.; Yu, M.J.; von Oheimb, G. Tree morphology responds to neighbourhood competition and slope in species-rich forests of subtropical China. *Forest Ecol. Manag.* **2010**, *260*, 1708–1715. [CrossRef]
38. Hu, S.S.; Ma, J.Y.; Shugart, H.H.; Yan, X.D. Evaluating the impacts of slope aspect on forest dynamic succession in Northwest China based on FAREAST model. *Environ. Res. Lett.* **2018**, *13*, 034027. [CrossRef]
39. Lu, D.S.; Mausel, P.; Brondizio, E.; Moran, E. Relationships between forest stand parameters and Landsat TM spectral responses in the Brazilian Amazon Basin. *Forest Ecol. Manag.* **2004**, *198*, 149–167. [CrossRef]

40. Barbosa, J.M.; Melendez-Pastor, I.; Navarro-Pedreno, J.; Bitencourt, M.D. Remotely sensed biomass over steep slopes: An evaluation among successional stands of the Atlantic Forest, Brazil. *ISPRS J. Photogramm. Remote Sens.* **2014**, *88*, 91–100. [CrossRef]
41. Rouse, J.W.; Haas, R.H.; Schell, J.A.; Deering, D.W. *Monitoring Vegetation Systems in the Great Plains with ERTS*; NASA: Washington, DC, USA, 1974.
42. Xiao, X.M.; Zhang, Q.Y.; Hollinger, D.; Aber, J.; Moore, B. Modeling gross primary production of an evergreen needleleaf forest using modis and climate data. *Ecol. Appl.* **2005**, *15*, 954–969. [CrossRef]
43. Geng, L.Y.; Che, T.; Ma, M.G.; Tan, J.L.; Wang, H.B. Corn Biomass Estimation by Integrating Remote Sensing and Long-Term Observation Data Based on Machine Learning Techniques. *Remote Sens.* **2021**, *13*, 2352. [CrossRef]
44. Hatton, N.M.; Menke, E.; Sharda, A.; van der Merwe, D.; Schapaugh, W. Assessment of sudden death syndrome in soybean through multispectral broadband remote sensing aboard small unmanned aerial systems. *Comput. Electron. Agric.* **2019**, *167*, 105094. [CrossRef]
45. Xue, J.R.; Su, B.F. Significant Remote Sensing Vegetation Indices: A Review of Developments and Applications. *J. Sens.* **2017**, *2017*, 1353691. [CrossRef]
46. Richardson, A.J.; Wiegand, C.L. Distinguishing Vegetation from Soil Background Information. *Photogramm. Eng. Remote Sens.* **1977**, *43*, 1541–1552.
47. Riitters, K.H.; Coulston, J.W. Hot spots of perforated forest in the eastern United States. *Environ. Manag.* **2005**, *35*, 483–492. [CrossRef]
48. Rogan, J.; Wright, T.M.; Cardille, J.; Pearsall, H.; Ogneva-Himmelberger, Y.; Riemann, R.; Riitters, K.; Partington, K. Forest fragmentation in Massachusetts, USA: A town-level assessment using Morphological spatial pattern analysis and affinity propagation. *GISci. Remote Sens.* **2016**, *53*, 506–519. [CrossRef]
49. Hernando, A.; Velazquez, J.; Valbuena, R.; Legrand, M.; Garcia-Abril, A. Influence of the resolution of forest cover maps in evaluating fragmentation and connectivity to assess habitat conservation status. *Ecol. Indic.* **2017**, *79*, 295–302. [CrossRef]
50. Sun, J.; Southworth, J. Indicating structural connectivity in Amazonian rainforests from 1986 to 2010 using morphological image processing analysis. *Int. J. Remote Sens.* **2013**, *34*, 5187–5200. [CrossRef]
51. Zhou, W.Q.; Zhang, S.; Yu, W.J.; Wang, J.; Wang, W.M. Effects of Urban Expansion on Forest Loss and Fragmentation in Six Megaregions, China. *Remote Sens.* **2017**, *9*, 991. [CrossRef]
52. Collinge, S.K. Ecological consequences of habitat fragmentation: Implications for landscape architecture and planning. *Landsc. Urban Plan* **1996**, *36*, 59–77. [CrossRef]